

BOOTSTRAP CURRENT IN QUASI-SYMMETRIC STELLARATORS

A. S. WARE* *University of Montana, Department of Physics and Astronomy, Missoula, Montana 59812*

D. A. SPONG, L. A. BERRY, S. P. HIRSHMAN, and J. F. LYON
Oak Ridge National Laboratory, Oak Ridge, Tennessee 37831-6169

Received December 5, 2005

Accepted for Publication February 9, 2006

This work examines bootstrap current in quasi-symmetric stellarators with a focus on the impact of bootstrap current on the equilibrium properties of stellarator configurations. In the design of the Quasi-Poloidal Stellarator (QPS), a code was used to predict the bootstrap current based on a calculation in an asymptotically collisionless limit. This calculation is believed to be a good approximation of the bootstrap current for low-collisionality plasmas but is expected to be higher than the actual bootstrap current for more collisional plasmas. A fluid moments approach has been developed to self-consistently calculate viscosities and neoclassical transport coefficients. The viscosities and transport coefficients can be used to calculate the bootstrap current for arbitrary collisionality and magnetic geometry. The bootstrap current calculations from the two codes were done for low-density, electron cyclotron-heated (ECH) plasmas and high-density, ion cyclotron-heated (ICH) plasmas for a range of configurations, and provide a benchmark for the moments code and a test of the range of validity of the collisionless code. In the configurations examined here, namely, QPS, the National Compact Stellarator Experiment, the Helically Symmetric Experiment, the Large Helical Device, and the Wendelstein-7X Stellarator, the bootstrap currents predicted from the two codes agree qualitatively for both ICH and ECH profiles.

KEYWORDS: *bootstrap current, stellarators, magnetic confinement*

I. INTRODUCTION

Bootstrap current in a toroidal confinement device changes the rotational transform profile. In a stellarator this can potentially have a large impact on the quality of magnetic surfaces, especially near the edge where the introduction of low-order rational surfaces can introduce islands or stochastic regions. It can also affect magneto-hydrodynamic stability by changing the radial location of low-order rational surfaces or by adding a current gradient-driven term to the energy principle. In recent stellarator experiments, the obtainable β has increased.^{1,2} Here, β is the ratio of the volume-averaged plasma pressure to the magnetic field strength squared. This trend will likely continue as stellarators currently under construction, namely, the National Compact Stellarator Experiment³ (NCSX) and the Wendelstein 7-X Stellarator⁴ (W7-X), have even higher β as operational goals. The higher β values in these experiments may lead to increased bootstrap current in these devices. Indeed, these devices, as well as the Quasi-Poloidal Stellarator⁵ (QPS), have bootstrap current constraints in their design optimization. Namely, the W7-X optimization minimized the bootstrap current, the NCSX optimization targeted bootstrap current similar to an axisymmetric device, and the QPS optimization targeted matching the bootstrap and plasma current required in the finite- β optimization. The impact of bootstrap current on reactor-size stellarators has also been examined.⁶ An improved understanding of bootstrap current in stellarators is therefore an important goal for theoretical research.

In the design of a number of these devices, the bootstrap current was estimated using a semianalytic formulation of the bootstrap current in an asymptotically collisionless limit.⁷ The BOOTSJ code uses this formulation to provide a rapid estimate of the bootstrap current that can be easily implemented in an optimization routine. Using the BOOTSJ code, the bootstrap current can

*E-mail: andrew.ware@umontana.edu

be calculated on every surface of a given equilibrium (approximately 50 surfaces) in less than a minute of CPU time on an IBM SP RS/6000. This calculation is believed to give an accurate prediction of the bootstrap current in a collisionless plasma and an overestimate in a collisional plasma. For QPS this implies an accurate prediction in the case of a high-electron temperature (T_e), low-density (n), electron cyclotron-heated (ECH) plasma ($n \sim 3 \times 10^{19} \text{ m}^{-3}$, $T_e \sim 1 \text{ keV}$, $T_i \sim 0.2 \text{ keV}$), and an overestimate for a lower T_e , high n , ion cyclotron-heated (ICH) plasma ($n \sim 8 \times 10^{19} \text{ m}^{-3}$, $T_e \sim 0.4 \text{ keV}$, $T_i \sim 0.4 \text{ keV}$). The degree of accuracy of this calculation has not previously been benchmarked against any other code. The collisionality at which the asymptotic limit breaks down is also not clear because of the uncertain effects of shallow wells.

A new moments method for calculating neoclassical transport has been developed.⁸ This method uses analytic formulations coupled with the results of the Drift Kinetic Equation Solver code⁹ (DKES). The moment method for neoclassical transport calculations was originally developed by Hirshman and Sigmar¹⁰ for axisymmetric geometry and was extended to three-dimensional geometry by Shaing and Callen.¹¹ Sugama and Nishimura¹² developed a method for calculating the transport coefficients numerically using DKES for three-dimensional configurations. The moments-based transport model allows for calculating plasma flows for arbitrary geometry and a range of collisionalities from lower plateau to lower Pfirsch-Schlüter. The bootstrap current is one of the quantities that can be determined from this transport model. The calculations presented in this paper provide a comparison between the BOOTSJ and moments-based transport model. This work is also complementary in nature to early work by Maassberg et al. that compared DKES results with a Monte Carlo code for a single optimized configuration.¹³

The remainder of this paper is organized as follows. In Sec. II, the equilibrium configurations and the plasma profiles are described. In Sec. III, results for both ECH and ICH plasmas are presented. In Sec. IV, the impact of the bootstrap current on the rotational transform is examined. Finally, in Sec. V, a brief discussion is presented.

II. EQUILIBRIA

In this work, five different configurations are considered including three recently designed stellarators, QPS, NCSX, and W7-X, and two existing experiments, the Large Helical Device¹⁴ (LHD) and the Helically Symmetric Experiment¹⁵ (HSX). Three of these are quasi-symmetric (namely, HSX is quasi-helically symmetric, NCSX is quasi-axisymmetric, and QPS is quasi-poloidally symmetric). The other two configurations are included for the sake of comparison. The effect of collisionality and the radial electric field on bootstrap current in LHD

TABLE I

Scaling Factors for the Size (Major Radius) and Magnetic Field Strength for Five Configurations

Device	R Scale Factor	$ \mathbf{B} $ Scale Factor
HSX	2.724	2.000
LHD	0.500	0.333
QPS	1.000	1.000
NCSX	1.042	0.608
W7-X	0.626	0.333

has previously been examined.¹⁶ Here, the focus will be the effect of the magnetic configuration on the bootstrap current. To focus on the effect of magnetic geometry, all configurations have been scaled to an average minor radius of $\langle a \rangle = 0.33 \text{ m}$ and an average magnetic field strength of $\langle |\mathbf{B}| \rangle = 1.0 \text{ T}$. These are typical values for QPS and imply a scaling of the other configurations as shown in Table I. The Variational Moments Equilibrium Code¹⁷ (VMEC) is used to calculate fixed-boundary equilibrium for these configurations. The outer flux surfaces of these scaled plasmas are shown in Fig. 1. These are vacuum flux surfaces ($\beta = 0$ and no plasma current) except for the NCSX case, which has 113 kA of toroidal plasma current. In the calculations of the bootstrap current below, it is these vacuum (non-self-consistent) fields that are used.

In the calculation of bootstrap currents, two separate sets of profiles for T_e , T_i (ion temperature), and n , associated with two different heating mechanisms, have been studied. Both use a broad density profile with pedestals in both density and temperature. Quasi-neutrality is assumed with $n_e = n_i = n$. The profiles for density and temperature are

$$n = n_0 \frac{[\delta_n + (1 - \rho^6)^2]}{1 + \delta_n} \quad (1)$$

and

$$T = T_0 \frac{[\delta_T + (1 - \rho^2)^2]}{1 + \delta_T}, \quad (2)$$

where $\rho = \sqrt{S}$ and S is the normalized toroidal flux, n_0 and T_0 are the density and temperature on axis, and δ_n and δ_T represent pedestal factors. For the ICH plasmas the parameters are $T_{i0} = 0.3 \text{ keV}$, $T_{e0} = 0.5 \text{ keV}$, $n_0 = 8.0 \times 10^{13} \text{ cm}^{-3}$, $\delta_n = 1.0$, and $\delta_T = 0.6$. For the ECH plasmas the parameters are $T_{i0} = 0.2 \text{ keV}$, $T_{e0} = 1.5 \text{ keV}$, $n_0 = 2.5 \times 10^{13} \text{ cm}^{-3}$, $\delta_n = 1.0$, and $\delta_T = 0.6$. The plasma profiles for density, electron temperature, and ion temperature are shown for both ICH and ECH in Fig. 2. The temperature and density profiles result in a zero-pressure

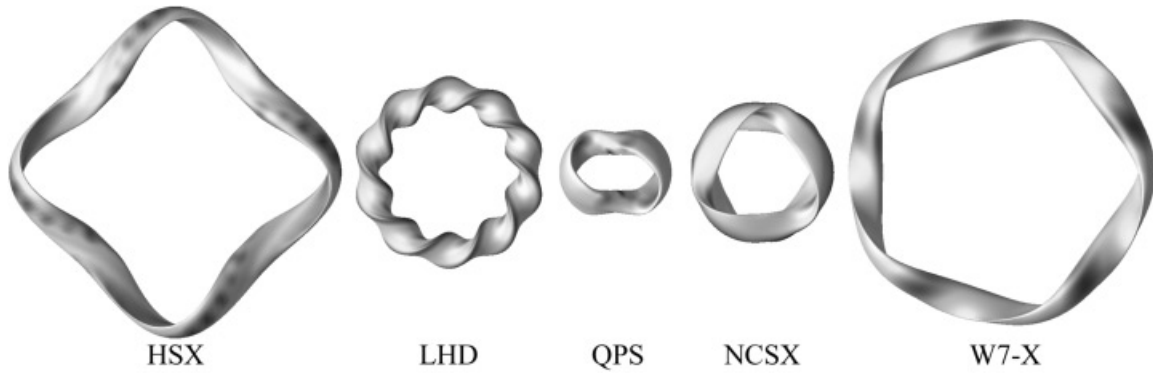


Fig. 1. Outer flux surface for the five configurations discussed in this paper: HSX, LHD, QPS, NCSX, and W7-X. All configurations have been scaled to $\langle a \rangle = 0.33$ m and $\langle |\mathbf{B}| \rangle = 1.0$ T. Darker regions on the surface indicate stronger magnetic field strength.

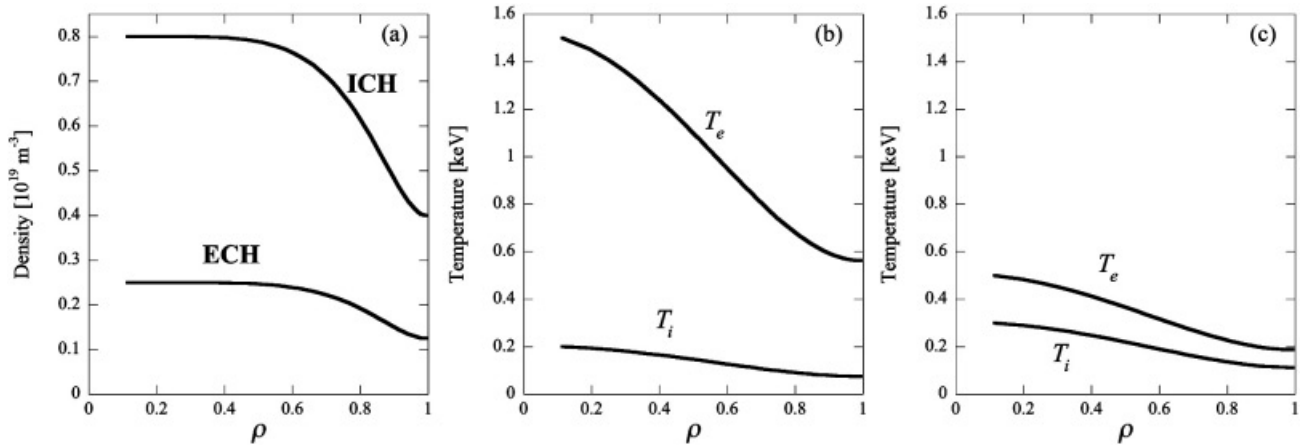


Fig. 2. Profiles of (a) the density for both the ICH and ECH cases, (b) the ion and electron temperature profiles for the ECH case, and (c) the ion and electron temperature profiles for the ICH case.

gradient at the edge ($\rho = 1$) thereby precluding the possibility of a discontinuity of the bootstrap current at the edge.

The normalized collisionality for these cases is $\nu^* = \nu R_0 / w_{th}$, where ν is the collisionality, R_0 is the average major radius, ι is the rotational transform, and w_{th} is the thermal velocity. The profiles of the ion and electron collisionalities are shown for the ECH cases in Figs. 3a and 3b and for the ICH cases in Figs. 3c and 3d. For the ECH cases, the electrons have a low collisionality ($\nu^* < 1$) over the whole cross section, especially for the W7-X and QPS configurations. For the ICH cases, in all the configurations the electrons have collisionality $\nu^* > 1$ over the majority of the cross section. For both the ECH and ICH cases, the ions have an effective collisionality $\nu^* > 1$ for all configurations. The self-consistent ambipolar radial electric field solutions from the moment-based method are shown in Fig. 4 (Ref. 18).

III. BOOTSTRAP CURRENT CALCULATIONS

Bootstrap current calculations in the moments-based model are performed including a self-consistent ambipolar electric field. The profiles discussed above were chosen in part to ensure a continuous electric field solution (i.e., no root-jumping or bifurcations) across the minor radius for all of the configurations examined. In the following, the BOOTSJ and moments model results are compared for collisional (ICH) and collisionless (ECH) plasmas. For the comparisons, the flux surface-averaged, field-aligned bootstrap current $\langle \mathbf{J}_{bs} \cdot \mathbf{B} \rangle$ is shown as a function of the normalized minor radius ρ .

The bootstrap current predictions with the ICH profiles from both the BOOTSJ and moments-based transport model are shown in Fig. 5. Even for these relatively collisional plasma parameters, the predictions of the two codes agree qualitatively, but there are some quantitative

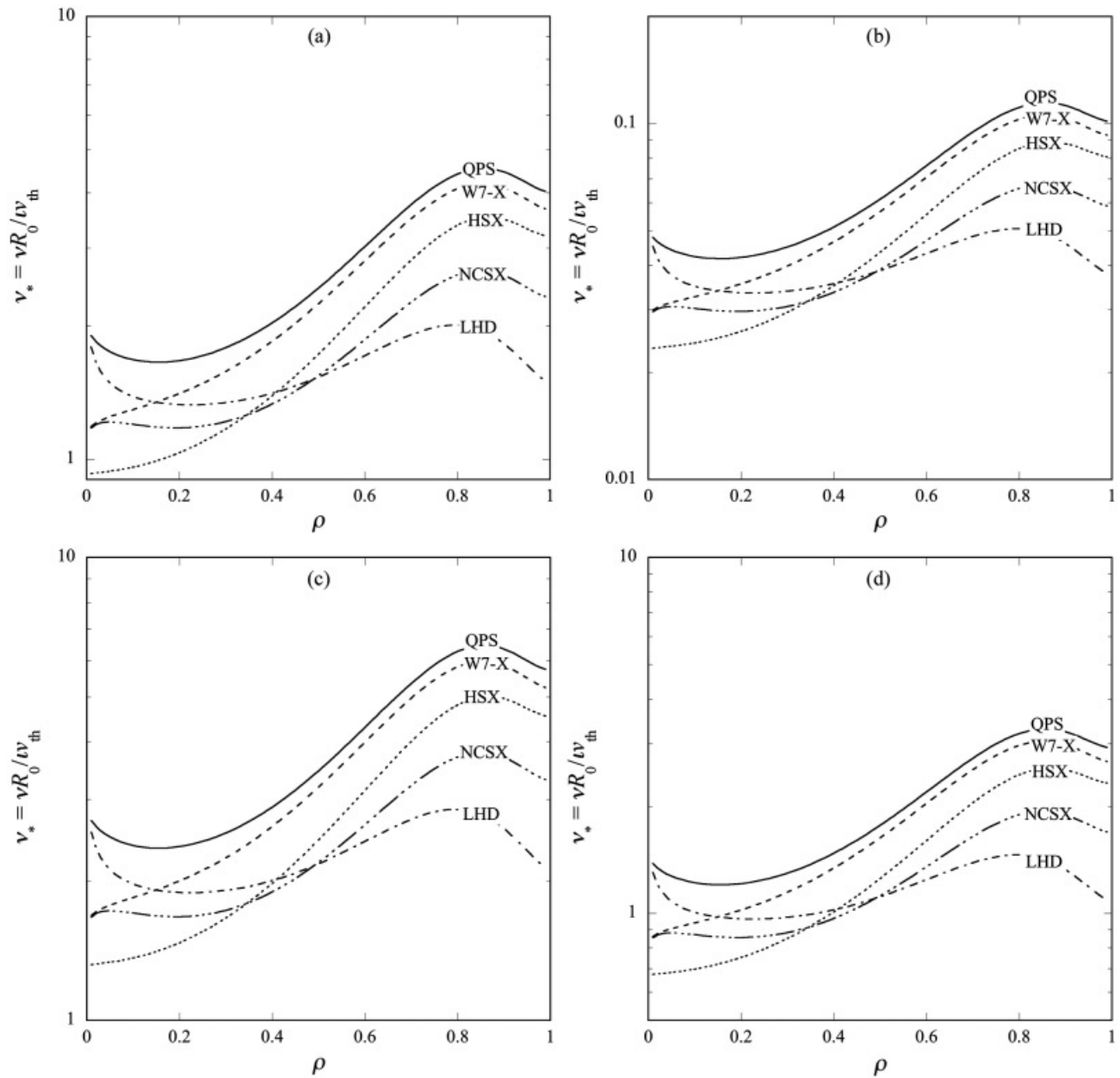


Fig. 3. Profiles of the normalized collisionality for (a) ions and (b) electrons in the ECH case and (c) ions and (d) electrons in the ICH case.

differences for the different configurations. The total bootstrap currents for these cases are shown in Table II. For the ICH cases, BOOTSJ predicts similar (LHD and QPS) or larger total currents (HSX, NCSX, and W7-X) compared to the moments-based model. The largest differences between the two models occur for the NCSX and W7-X configurations for which the moments model predicts a larger bootstrap current by a factor of 1.7 and 2.4, respectively. The BOOTSJ code has resonances at lower-order rational surfaces. The examples of these are the small jumps in the profile for NCSX and the large

drop in the profile for HSX as shown in Fig. 5. The drop in the HSX bootstrap current profile occurs near the $\rho = 0.74$ surface where the rotational transform is 0.222 and the jump is likely associated with an 8/9 resonance.

The bootstrap current predictions with the ECH profiles from both the BOOTSJ and moments-based transport model are shown in Fig. 6. Here, less surprisingly, the results agree qualitatively, but again there are quantitative differences between the results from the two codes for different configurations. The total bootstrap currents for these cases are also shown in Table II. For

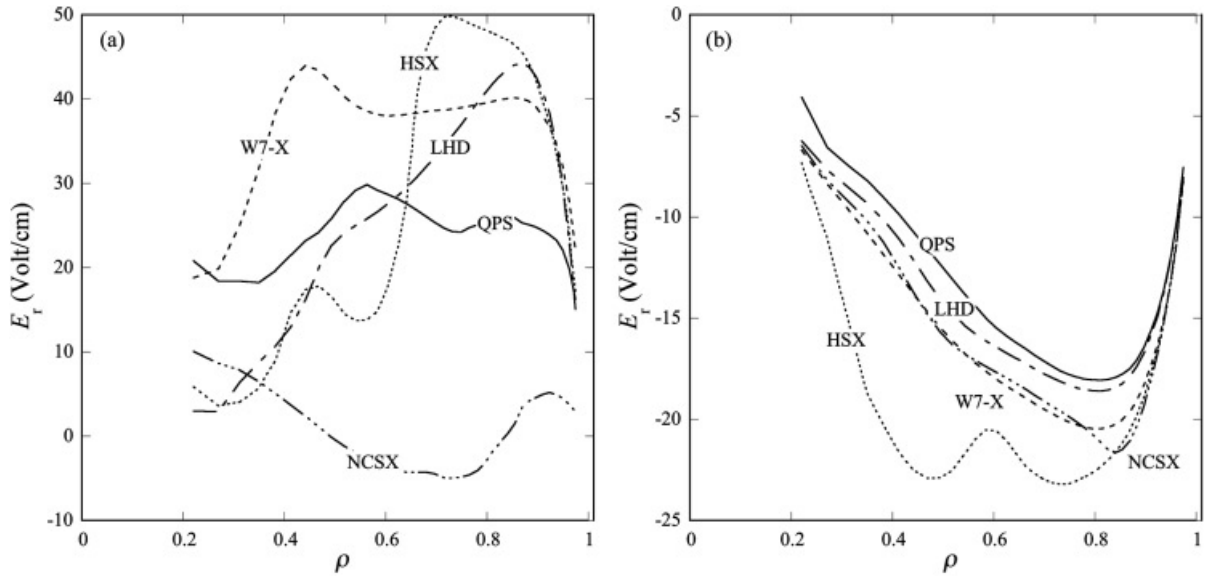


Fig. 4. Profiles of the ambipolar radial electric field used in the moments-based transport model for (a) the ECH case and (b) the ICH case.

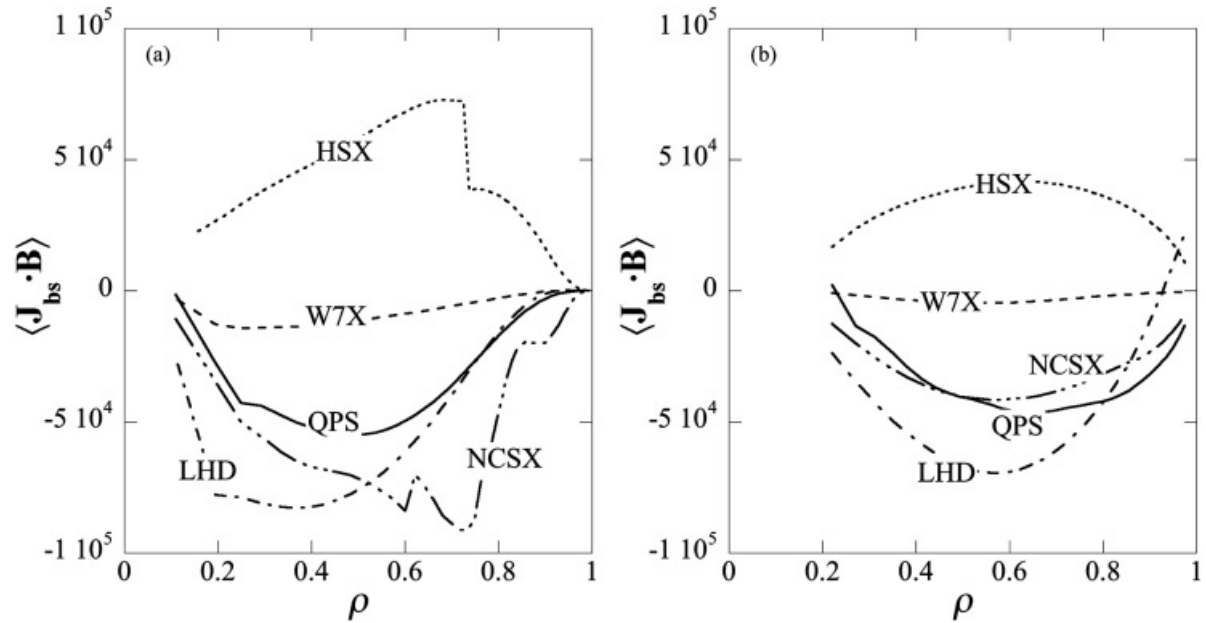


Fig. 5. Magnetic-field-aligned bootstrap current profile for five different configurations with the same high-collisionality ICH profiles shown in Fig. 1 as predicted by (a) the BOOTSJ code and (b) the moments-based transport model. The field-aligned current is in units of $A \cdot T/m^2$.

the ECH cases, BOOTSJ predicts lower total bootstrap current compared to the moments model for all the configurations except for W7-X (both models, however, do predict a small total current for W7-X). The largest difference is for QPS: The moments model predicts a boot-

strap current three times that predicted by the BOOTSJ code. This is primarily due to a second peak of the bootstrap current profile as predicted by the moments model that does not correspond to a feature in the density, temperature, or collisionality profiles.

TABLE II
Total Bootstrap Current Predicted from the BOOTSJ
and Moments Model for Five Configurations

Device	I_{bs} (ECH) (kA)		I_{bs} (ICH) (kA)	
	BOOTSJ	Moments	BOOTSJ	Moments
HSX	9.5	15.2	12.4	9.7
LHD	9.1	11.5	12.0	12.3
QPS	6.5	18.4	8.8	10.4
NCSX	12.0	16.4	15.8	9.1
W7-X	1.4	0.8	1.9	0.8

IV. EFFECT OF THE BOOTSTRAP CURRENT ON THE ROTATIONAL TRANSFORM

The bootstrap current can impact equilibrium, transport, and stability properties of toroidal plasmas. Of these, often the most direct impact is on the rotational transform. Three-dimensional equilibria can often be sensitive to changes in the rotational transform profile due to the possible presence of islands on low-order rational surfaces near the edge region. To test the impact of the predicted bootstrap currents on the equilibrium properties, new equilibria for three of these cases were calculated with current profiles that match the predicted bootstrap profiles from the BOOTSJ code for the ECH cases. Note that these are not self-consistent profiles but current profiles that match the bootstrap current predicted from *vacuum* magnetic fields.

Figure 7a shows the predicted bootstrap current for ECH in W7-X and the plasma current from VMEC for a W7-X equilibrium with a matching plasma current, and Fig. 7b shows the rotational transform profiles for these two cases (i.e., in vacuum and with plasma current). The total plasma current for this case is 1.4 kA. The impact of this current on the rotational transform is a small increase in the core region but almost no change near the edge. This is an important result for the planned operation of W7-X with an island divertor outside the last closed flux surface.

Figure 8a shows the predicted bootstrap current for ECH in QPS and the plasma current from VMEC for a QPS equilibria with a matching plasma current, and Fig. 8b shows the rotational transform profiles for these two cases. The total plasma current for this case is 6.5 kA. There is an increase of rotational transform across the entire cross section with this amount of plasma current. Indeed, QPS was designed with the expectation that plasma current, including self-consistent bootstrap current, will provide a portion of the total rotational transform¹⁸ (this is also the case for NCSX). Since QPS has lower rotational transform relative to most other stellarators, additional rotational transform can be a beneficial result of bootstrap

current in QPS. While no bootstrap current is expected for a truly poloidally symmetric stellarator, this is not possible for a realizable stellarator configuration. The bootstrap current naturally tends to be larger at lower-plasma-aspect ratio and has been chosen to satisfy other optimization criteria for QPS. The impact of adding 9.1 kA of current to the LHD equilibrium has a similar impact on its rotational transform, namely, a small increase in the transform in the central region with almost no change at the plasma edge.

Figure 9a shows the predicted bootstrap current for ECH in HSX and the plasma current from VMEC for an HSX equilibrium with a matching plasma current, and Fig. 9b shows the rotational transform profiles for these two cases. The total plasma current for this case is 9.5 kA. For HSX, there is a large decrease in the rotational transform due to the bootstrap current. The rotational transform profile shifts from weak, stellarator shear in vacuum to a reversed shear profile that crosses the $\iota = 1$ surface twice. This can result in possible degradation of the equilibrium and stability properties of HSX. For a quasi-helically symmetric device to operate at significant β , external current drive to maintain control over the magnetic configuration may be required.

Finally, for the NCSX configuration, the equilibrium current is 113 kA. That implies the 12 kA of bootstrap current would need to be augmented by external current drive to achieve this configuration. The actual NCSX experiment is expected to run at higher β and lower collisionality, thereby producing more bootstrap current than predicted here.

V. DISCUSSION

The bootstrap current calculations discussed here show that there is qualitative agreement between the bootstrap current predicted by the BOOTSJ code and the moments model. The level of quantitative difference between the predictions from the two codes is dependent on the magnetic configuration. For the quasi-symmetric configurations, the moments model predicts >50% more bootstrap current in the ECH cases compared to the ICH cases. For the other two configurations discussed here, the moments model predicts roughly the same bootstrap current for both the ECH and ICH cases. The BOOTSJ code predicts roughly one-third more current in the ICH cases compared to the ECH cases for all of the configurations.

For the ECH and ICH cases discussed here, there is no clear “scaling factor” that can be used to correct the BOOTSJ results for a higher-collisionality plasma. It is true, however, that the differences between the BOOTSJ predictions and the moments model are, in general, larger for the configurations with lower effective collisionality (namely, W7-X and QPS).

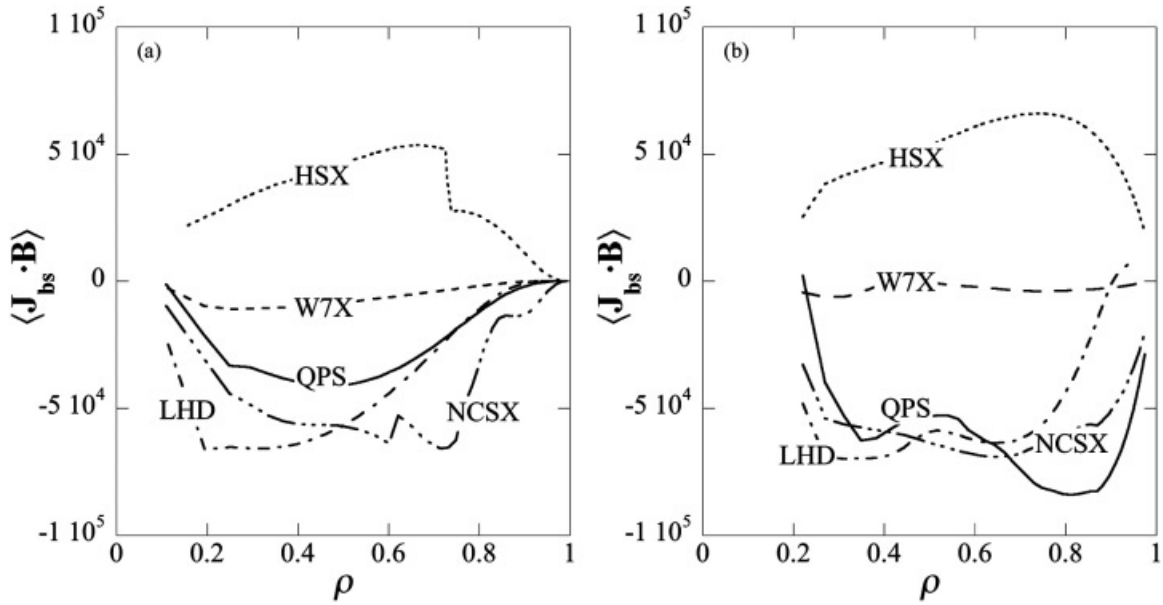


Fig. 6. Magnetic-field-aligned bootstrap current profile for five different configurations with the same low-collisionality ECH profiles shown in Fig. 1 as predicted by (a) the BOOTSJ code and (b) the moments-based transport model.

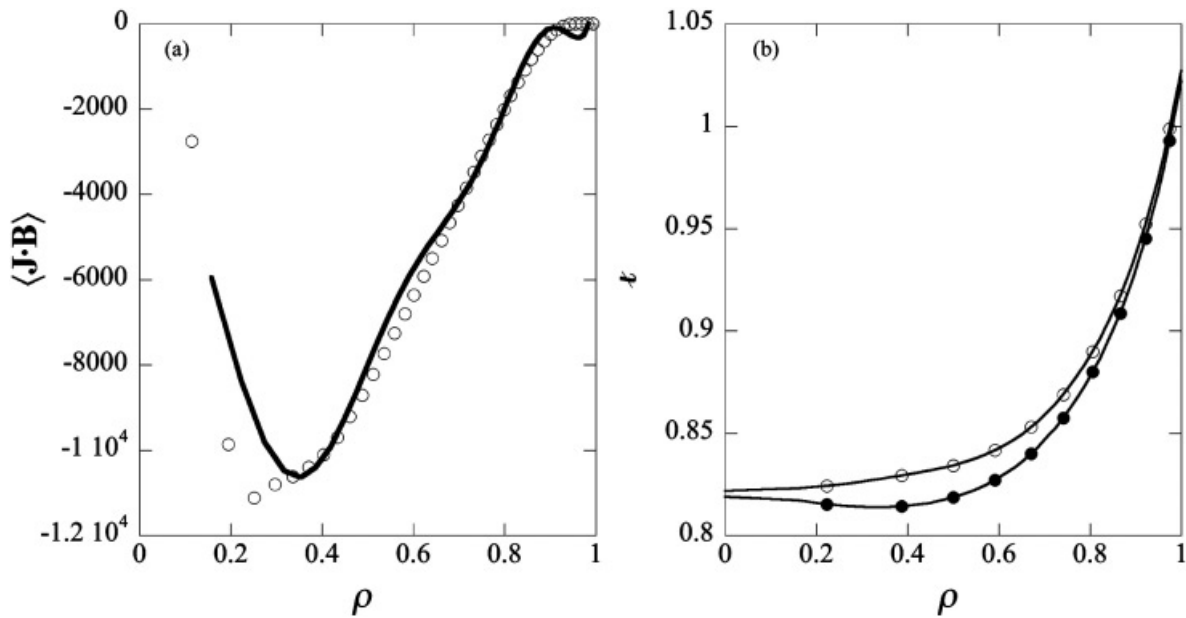


Fig. 7. (a) Bootstrap current predicted by BOOTSJ for W7-X vacuum fields with ECH profiles (open circles) and plasma current from VMEC for a W7-X equilibrium with 1.4 kA of plasma current (solid line). (b) Rotational transform profiles for the vacuum (closed circles) and with current cases (open circles) for W7-X.

The level of bootstrap current predicted by these codes affects the rotational transform profile. The bootstrap current is, as expected, smallest in the W7-X configuration and has a correspondingly small effect on the rotational transform profile. The bootstrap current adds

to the vacuum rotational transform in the LHD, NCSX, and QPS configurations. In the HSX configuration, the bootstrap current reduces the vacuum rotational transform. It should be noted that these are not self-consistent bootstrap currents. These current profiles are based on

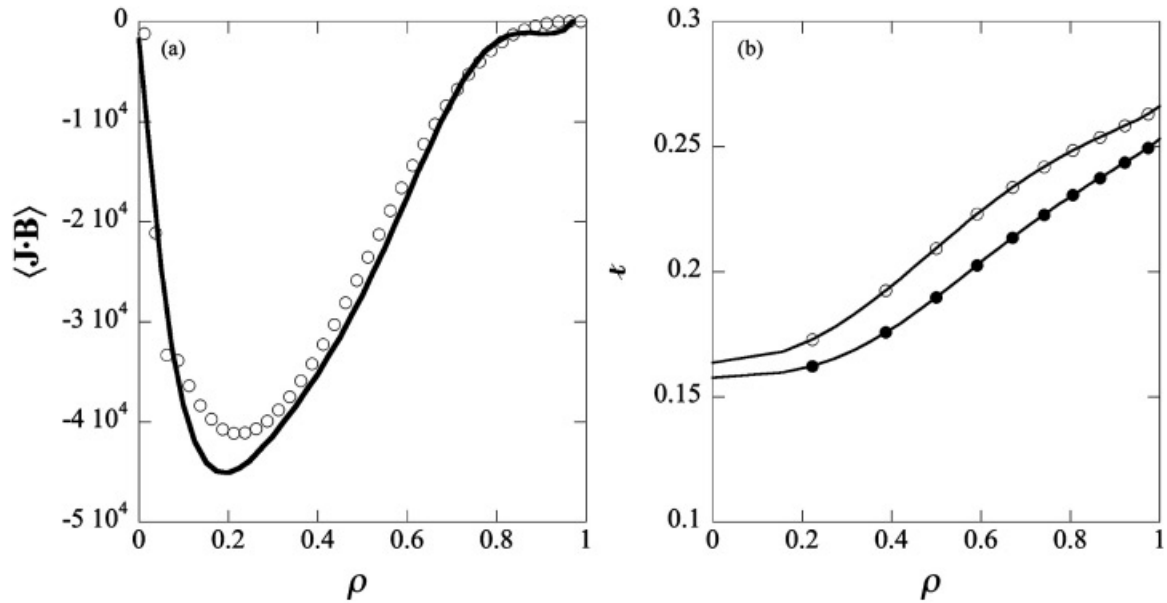


Fig. 8. (a) Bootstrap current predicted by BOOTSJ for QPS vacuum fields with ECH profiles (open circles) and plasma current from VMEC for a QPS equilibrium with 6.5 kA of plasma current (solid line). (b) Rotational transform profiles for the vacuum (closed circles) and with current cases (open circles) for QPS.

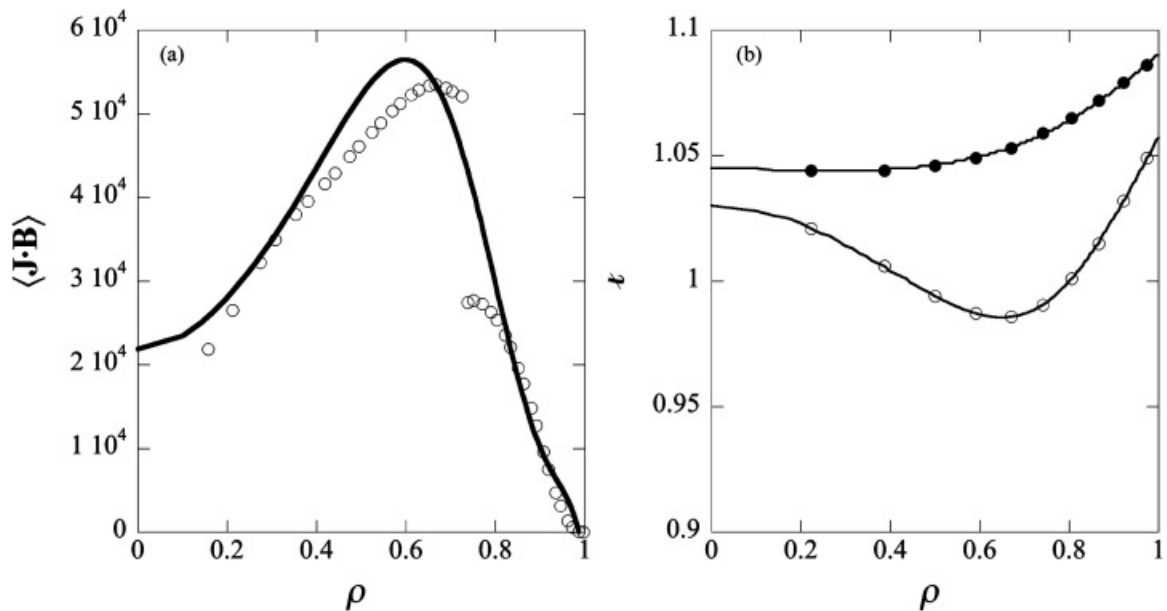


Fig. 9. (a) Bootstrap current predicted by BOOTSJ for HSX vacuum fields with ECH profiles (open circles) and plasma current from VMEC for an HSX equilibrium with 9.5 kA of plasma current (solid line). (b) Rotational transform profiles for the vacuum (closed circles) and with current cases (open circles) for HSX.

the vacuum magnetic configuration. The results presented here are only an indication of the impact of bootstrap current on the rotational transform in these devices. Equilibria with self-consistent bootstrap current have been calculated for some of these configurations [e.g., NCSX (Ref. 3) and QPS (Ref. 19)].

ACKNOWLEDGMENTS

This research was supported by the U.S. Department of Energy under grant DE-FG 03-97ER54423 at the University of Montana and under contract DE-AC05-00OR22725 at Oak Ridge National Laboratory, managed by UT-Battelle, LLC. This research used resources of the National Energy Scientific

Computing Center, which is supported by the Office of Science of the U.S. Department of Energy under contract No. DE-AC03-76SF00098.

REFERENCES

1. K. McCORMICK et al., *Phys. Rev. Lett.*, **89**, 015001 (2002).
2. O. MOTOJIMA et al., *Nucl. Fusion*, **43**, 1674 (2003).
3. M. C. ZARNSTORFF et al., *Plasma Phys. Control. Fusion*, **43**, A237 (2001).
4. C. BEIDLER et al., *Fusion Technol.*, **17**, 148 (1990).
5. D. J. STRICKLER et al., *Fusion Sci. Technol.*, **45**, 15 (2004).
6. S. F. MARGALET et al., *Fusion Sci. Technol.*, **46**, 44 (2004).
7. K. C. SHAINING et al., *Phys. Fluids B*, **1**, 148 (1989).
8. D. A. SPONG, *Phys. Plasmas*, **12**, 056114 (2005).
9. W. I. VAN RIJ and S. P. HIRSHMAN, *Phys. Fluids B*, **1**, 563 (1989).
10. S. P. HIRSHMAN and D. J. SIGMAR, *Nucl. Fusion*, **21**, 1079 (1981).
11. K. C. SHAINING and J. D. CALLEN, *Phys. Fluids*, **26**, 3315 (1983).
12. H. SUGAMA and S. NISHIMURA, *Phys. Plasmas*, **9**, 4637 (2002).
13. H. MAASSBERG, W. LOTZ, and J. NÜHRENBERG, *Phys. Fluids B*, **5**, 3728 (1993).
14. A. IIYOSHI et al., *Fusion Technol.*, **17**, 169 (1990).
15. F. S. B. ANDERSON et al., *Fusion Technol.*, **27**, 273 (1995).
16. K. Y. WATANABE et al., *Nucl. Fusion*, **35**, 335 (1995).
17. S. P. HIRSHMAN and J. C. WHITSON, *Phys. Fluids*, **26**, 3553 (1983).
18. D. A. SPONG, "Sheared Plasma Flow Generation: A New Measure for Stellarator Optimization," *Fusion Sci. Technol.*, **50**, 3 (2006).
19. D. A. SPONG et al., *Nucl. Fusion*, **41**, 711 (2001).